ACS OMEGA

Article

Cite This: ACS Omega 2018, 3, 112−123

Nanocapillarity and Liquid Bridge-Mediated Force between Colloidal Nanoparticles

Luis G. MacDowell,*[,†] Pablo Llombart,[†] Jorge Benet,[†] Jose G. Palanco,[‡] and Andrés Guerrero-Martinez[†]

[†]Departamento de Química Física, Facultad de Ciencias Químicas, Universidad Complutense, Avda. Complutense s/n, 28040 Madrid, Spain

[‡]Departamento de Materiales y Producción Aeroespacial, ETSI Aeronáuticos, Universidad Politécnica de Madrid, Plaza del Cardenal Cisneros 3, 28040 Madrid, Spain

ABSTRACT: In this work, we probe the concept of interface tension for ultrathin adsorbed liquid films on the nanoscale by studying the surface fluctuations of films down to the monolayer. Our results show that the spectrum of film height fluctuations of a liquid−vapor surface may be extended to ultrathin films provided we take into account the interactions of the substrate with the surface. Global fluctuations of the film height are described in terms of disjoining pressure, whereas surface deformations that are proportional to the interface area are accounted for by a film thickness-dependent surface tension. As a proof of concept, we model the capillary forces between colloidal nanoparticles held together by liquid bridges. Our results indicate that the classical equations for capillarity follow very precisely down to the nanoscale provided we account for the film height dependence of the surface tension.

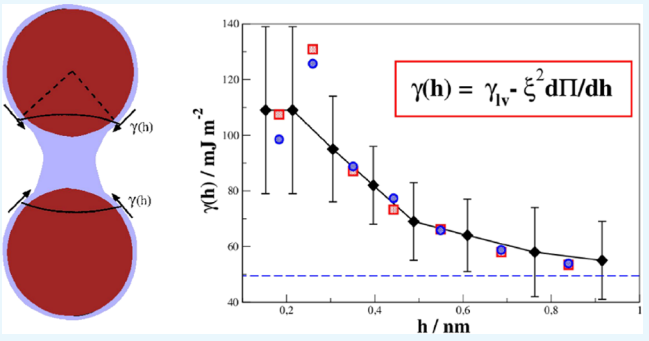

INTRODUCTION

If one studies monolayer formation on droplets,[1] evaporative colloidal deposition,[2,3] the buoyancy of suspended particles on an interface,[4] or the aggregation of colloidal nanoparticles by capillary condensation,[5] most likely, the behavior of the system can be explained in terms of capillarity theory.[6,7] At the heart of this approach lies the approximation that bulk and surface properties of large planar bodies can be extrapolated to describe small and curved systems. Such is the case of the Young−Laplace equation relating the curvature κ of a curved interface with the bulk pressure difference between the liquid and vapor phases, Δp, and the interface tension, γ_{lv}, that is, $\Delta p = \gamma_{lv}\kappa$. This result, namely, that films and interfaces adopt shapes of constant curvature has been tested and proved for a wide range of situations in systems from the millimeter to the micrometer range.[7] However, as the scale of systems decreases below micrometers, phenomenological corrections for the macroscopic properties are required and concepts such as line tension and Tolman length need to be introduced.[8] These corrections indicate the presence of intermolecular forces with a range that approaches the scale of the problem in hand.[9]

In the study of adsorption, thin liquid films of a few-nanometer thickness fall in this group. The liquid−vapor interface of the adsorbed film feels interactions from the substrate, and the force balance embodied in the Laplace equation no longer holds. The missing link required to re-establish the mechanical equilibrium in such cases is the celebrated concept of disjoining pressure, $\Pi(h)$,[10] which measures the forces exerted by the substrate on a film of height $h(\mathbf{x})$ above a point $\mathbf{x}$. This leads to the Young−Laplace−Derjaguin equation of thin adsorbed films:[6,7]

$$\Delta p = \gamma_{lv}\kappa - \Pi(h) \tag{1}$$

This result has been employed ubiquitously to describe the average shape and forces of colloidal systems in the nanometer range.[11,12] However, intrinsic to systems of small size is the presence of large thermodynamic fluctuations. These become important on the nanoscale because large deviations from the average have only a small free energy penalty relative to the most stable state. In such cases, it is convenient to have at hand a way to assess the relative probabilities of the most significant fluctuations.[13]

In thin liquid films, precisely, this goal may be accomplished using interface Hamiltonians borrowed from the field of surface physics. Here, one considers not the force balance but rather the free energy cost of specific realizations of the film profile, $h(\mathbf{x})$, which, for adsorbed films, may be conveniently cast as

$$H[h] = \int d\mathbf{x}[g(h) + \gamma_{lv}\sqrt{1 + (\nabla h)^2} - \Delta p h] \tag{2}$$

where $g(h)$ is the interface potential or free energy of a planar film of height h above a substrate, with $\Pi(h) = -dg(h)/dh$, and

Received: October 26, 2017
Accepted: December 21, 2017
Published: January 5, 2018

DOI: 10.1021/acsomega.7b01650
ACS Omega 2018, 3, 112−123

the integration is carried out over a flat reference plane with a coordinate **x** (Monge representation). The minimization of this functional with respect to the film profile provides exactly eq 1 for the equilibrium condition of a film, but the integrated form mentioned above allows also the assessment of the free energy cost of fluctuations.

In fact, the partition function of this Hamiltonian may be solved in the limit of small gradients by expanding the film height in surface Fourier modes, $h(\mathbf{q})$, with $\mathbf{q}$, a vector in the reciprocal space of **x**. It is then possible to calculate the free energy cost of fluctuations disturbing locally the surface height away from the average equilibrium value, h_e. This yields an equation for the mean-squared amplitude of surface Fourier modes as[9,14−16]

$$\langle |h(\mathbf{q})|^2 \rangle = \frac{k_B T}{A(g''(h_e) + \gamma_{lv} q^2)} \tag{3}$$

where $g''(h) = -\mathrm{d}\Pi/\mathrm{d}h$ is given by the derivative of Π with respect to h and A is the lateral area. This result indicates that the spectrum of surface fluctuations provides interesting information on the properties of the adsorbed liquid−vapor interface, γ_{lv}, as well as on the molecular forces that tie it to the substrate, $g''(h)$. Indeed, using X-ray surface scattering techniques, it is possible to probe the related *parallel correlation length*, $\xi_\parallel^2 = \gamma_{lv}/g''(h_e)$, which corresponds to the familiar capillary length for interfaces subject to gravity.[17] A number of experiments performed for thin films of several-nanometer thickness confirm that $\xi_\parallel^2 \propto h_e^4$, as expected for wetting films governed by van der Waals interactions, where $\Pi(h) = -\frac{A_w}{6\pi h^3}$, with A_w being the Hamaker constant. However, it has been proved far more difficult to confirm that the coefficient of q^2 in eq 3 is precisely equal to the liquid−vapor surface tension, with conflicting results found in the literature.[18−20]

Recently, we have performed computer simulation studies of thin adsorbed films subject to van der Waals forces.[16,21,22] Our calculations indicate that the results for $\Pi(h)$ obtained from the spectrum of surface fluctuations are in very good agreement with independent estimates for the disjoining pressure calculated by means of thermodynamic integration. However, we have found that an accurate agreement with eq 3 can only be recovered if we accept a film height-dependent surface tension, $\gamma(h)$, which becomes equal to γ_{lv} for sufficiently large $\gamma(h)$.[16,21−23] In fact, we have argued and shown empirically that decay of $\gamma(h)$ toward γ_{lv} is given in terms of disjoining pressure as[16,21−23]

$$\gamma(h) = \gamma_{lv} - \xi_e^2 \frac{\mathrm{d}\Pi(h)}{\mathrm{d}h} \tag{4}$$

where ξ_e is a parameter describing the width of the liquid−vapor interface. This result is consistent with previous unexplained computer simulation results[15] and with theoretical results for simplified models.[24] It should be noted that such a simple dependence is warranted only for systems that are dominated by long-range van der Waals interactions and does not hold in systems where the source of the disjoining pressure is given by structural contributions.

According to linear response theory, the spectrum of surface fluctuations is related to the response of the surface to external perturbations.[14] This means that eq 4 is not merely a minor correction required to describe the spectrum of surface fluctuations in detail but rather it accounts for substrate−film interactions that become relevant for sufficiently thin films and that are missed altogether in the Young−Laplace−Derjaguin equilibrium condition of eq 1. Unfortunately, the significance of a film height-dependent surface tension in capillarity theory beyond its signature in the capillary wave spectrum has not been tested to date. In this work, we will analyze the recent results for the force between titanium dioxide nanospheres joined by capillary bridges to assess the role of the film height-dependent surface tension.

In the next section, we provide an overview of a number of simulation techniques that have been employed in our laboratory to study and characterize model systems, which include the calculation of bulk-phase diagrams, interface potentials, and capillary wave fluctuations. We apply them here to obtain a detailed characterization of a well-known model of argon adsorbed on a solid carbon dioxide substrate. In the next section, we discuss the prewetting behavior of this system and exploit our results to illustrate the film height dependence of the surface tension. We then exploit our theoretical results for the film height-dependent surface tension of flat films to model capillary forces of curved interfaces in liquid bridges. We end our paper with a discussion on the significance of our results.

CHARACTERIZATION OF ADSORBED INTERFACES USING COMPUTER SIMULATIONS

In this section, we provide an overview of a number of computer simulation techniques that are useful to describe the wetting behavior of adsorbates on model substrates. We first discuss the molecular model of argon adsorbed on CO_2 used in this work and studied extensively in the literature.[25−34] We then provide details of the calculation of its full bulk-phase diagram. This allows us to put into context the prewetting line reported previously.[32] We then calculate the interface potential of this system at a temperature slightly above the wetting temperature but yet safely above the triple point, in a region where the system exhibits prewetting. In such cases, the system can form metastable thick films. Finally, we describe how to calculate the surface tension of such films from an analysis of the capillary wave fluctuations. This will allow us to identify a film thickness-dependent surface tension and confirm the validity of an approximate theory meant to describe such dependence for thick films under the effect of long-range van der Waals forces.

Model and Simulations. The energy of interaction between two particles separated by a distance r is evaluated by the truncated Lennard-Jones (LJ) 12-6 potential.

$$u(r) = \begin{cases} 4\epsilon\left[\left(\frac{\sigma}{r}\right)^{12} - \left(\frac{\sigma}{r}\right)^{6}\right] & r \le R_c \\ 0 & r > R_c \end{cases} \tag{5}$$

where ϵ and σ are the energy and range parameters of the model, respectively, and $R_c = 2.5\sigma$ is the cutoff radius. Their corresponding values for argon are $\epsilon/k_B = 119.8$ K and $\sigma = 3.40$ Å.

The energy of interaction between the adsorbing wall and fluid particles a distance z away is evaluated by a long-range 9-3 potential:

$$u(z) = \frac{2\pi}{3}\rho_w \sigma_w^3 \epsilon_w \left[\frac{2}{15}\left(\frac{\sigma_w}{z}\right)^9 - \left(\frac{\sigma_w}{z}\right)^3\right] \tag{6}$$

DOI: 10.1021/acsomega.7b01650
ACS Omega 2018, 3, 112−123

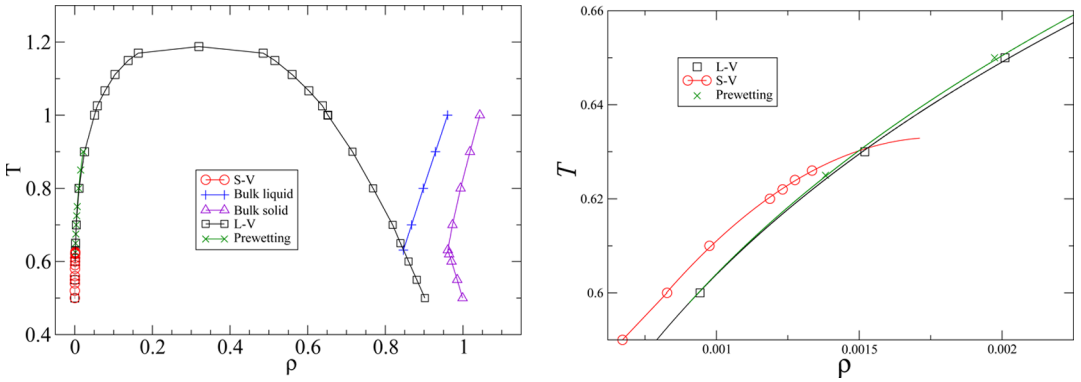

Figure 1. Bulk and wetting phase diagram for argon adsorbed on carbon dioxide. A) Bulk phase diagram of argon in the temperature−density plane. B) Detailed description of the liquid−vapor, solid−vapor and prewetting lines in the neighborhood of the triple point.

where, for the system Ar/CO_2, the parameter values are σ_w = 3.727 Å, ϵ_w/k = 153 K, and $\rho_w\sigma_w^3$ = 0.988. This choice of parameters was adopted in the seminal work of Ebner and Saam on the prewetting transition and later adopted with a cutoff radius of R_c = 2.5 Å by Finn and Monson.[25,35] It has been thereof a standard model for the study of wetting in both simulation studies and theoretical calculations.[27,30−32,36]

From now on, dimensionless quantities will be used, being ϵ and σ the characteristic units for energy and length, respectively.

Phase Diagram. Despite the previous calculations of the triple point for the full LJ potential[37,38] and the truncated and shifted LJ potential $R_c = 2.5\sigma$,[34,39] we were unable to find the corresponding result for the truncated LJ without the shift that is employed in this work.

This is an important matter as regards our study because the wetting temperature of the LJ fluid on our model substrate is very low, $k_BT_w = 0.60\epsilon$.[32] We can therefore not rule out that it corresponds to the wetting of a metastable liquid phase below the triple point, a situation that is known under the name of triple-point wetting.[40] For this reason, we calculated the full phase diagram, as indicated in the Methods section.

Figure 1a shows the complete LJ phase diagram obtained from our results. Figure 1b is an enlarged view in the neighborhood of the triple point. Using the prewetting chemical potentials reported by Errington,[32] which are in excellent agreement with our own results, we calculated the prewetting vapor densities from the virial equation of state. The region where the vapor and prewetting densities meet is shown in Figure 1b and clearly indicates a wetting temperature, k_BT_w = 0.60ϵ, which is below the bulk triple point, k_BT_t = 0.631ϵ.

This behavior is coincident with that observed by Toxvaerd for the truncated and shifted LJ and also corresponds to the experimental observation for Ar on solid CO_2[41] and the theoretical predictions.[36]

These results are an interesting case of metastability in small systems. In principle, it is not possible to measure the wetting temperature directly in a system exhibiting triple-point wetting. Below the triple point, the liquid−vapor coexistence curve is inside the region of stability of the solid phase. Accordingly, the system freezes before it is possible to observe the liquid phase wetting the substrate. Experimentally, triple-point wetting is often evidenced as the sudden wetting of a substrate as the vapor phase is heated across the triple point.[41−43]

Surprisingly, both Errington and ourselves could perform extremely long grand canonical simulations displaying the growth of a wetting liquid film at $k_BT = 0.60\epsilon$ (below the bulk triple point of the model LJ fluid) without any evidence of freezing.[21,32] Two possible reasons for this observation are as follows: (i) kinetically, a fast removal/insertion in the grand canonical simulations interferes with a slow nucleation process of the solid phase (ii) and thermodynamically, the limited system sizes and film heights studied could result in stabilization of the liquid film in regions where the bulk liquid phase is metastable.[40,42] Interestingly, a series of NVT simulations that were subsequently performed suggest that both reasons could be in play. Indeed, for sufficiently lengthy NVT simulation and sufficiently large film heights (of about $h > 6\sigma$), the layered liquid profiles developed gradually very strong peaks resembling a solid phase. This behavior was not found at all for thin films. A plausible interpretation is that in the latter, the liquid phase is still favored, even below the triple point, because of the influence of the wall−substrate interaction.[40,42] As the adsorbed phase becomes macroscopically large, however, it cannot possibly remain in the liquid phase and the film freezes. Because, possibly, the freezing is kinetically very slow and occurs only for thick enough films, as indicated by the NVT simulations, it is completely inhibited in the grand canonical simulations, which tunnel back and forth from thick to thin films and never give the thick films sufficient time to freeze.

Although this explanation seems plausible, further work is needed to clarify the stability of the wetting liquid phases simulated previously at $k_BT = 0.60\epsilon$.

Interface Potential. In mean field theory, the interface potential, $g(h)$, measures the free energy of a flat film of height h. In previous work,[44,45] we simply have assumed that the film height could be read off directly as a mass balance from the excess adsorbed number of molecules, whence $N_{ex} = A(\rho_l - \rho_v)h$. However, in the course of the simulations, the films are never strictly flat but rather exhibit capillary wave fluctuations. Therefore, the instantaneous film profile is best defined as a function $h(\mathbf{x})$. In this work, it is precisely the fluctuations of this instantaneous film height profile that we will use to probe the interface. Therefore, it is convenient to use here a measure of the average film height of a flat film that is consistent with the one we will use to measure surface fluctuations. In the next section, we will discuss the intrinsic sampling method (ISM) employed in this work to describe the local film height profile $h(\mathbf{x})$ in more detail.[46] For the time being, it suffices to assume that for a system with N molecules and surface area, A, inside

DOI: 10.1021/acsomega.7b01650
ACS Omega 2018, 3, 112−123

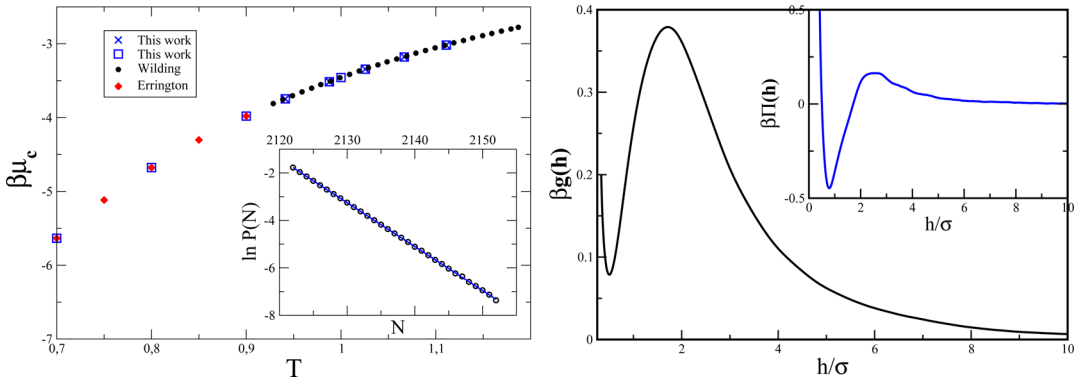

Figure 2. Calculation of the interface potential. (a) Coexistence chemical potential as a function of temperature as determined from this work for systems of size 10 × 10 × 20 (crosses) and 13 × 13 × 42 (squares). The results are compared with the equal area rule at high (circles[47]) and low temperatures (diamonds[32]). The inset shows the results of ln $P(N)$ as a function of N for a liquid slab in a simulation box of a lateral side of 13 × 13σ and a perpendicular distance of 42σ, simulated off coexistence at a temperature T = 0.9412 and a chemical potential $\beta\mu_0$ = −3.9312. The symbols fit to a straight line with a slope of −0.18502, which subtracted to $\beta\mu_0$ provide $\beta\mu_c$ = −3.74613 in excellent agreement with the method of equal area rule. (b) Interface potential for Ar(g) adsorbed on a substrate at a temperature above the wetting point. A metastable minimum can be observed. Inset: corresponding disjoining pressure isotherm obtained upon numerical differentiation of the interface potential.

volume V, there is a uniquely defined canonically averaged film height for each N, as

$$h = \langle h(\mathbf{x}) \rangle_{\mathbf{x}\mathrm{NVT}} \tag{7}$$

where the subscript indicates both lateral and canonical averages. In essence, this is simply a convenient way to express the average adsorption in units which roughly indicate the thickness of the adsorbed film.

Notice that such a definition coarsens the fluctuations of the film height at fixed N. For example, one could envisage situations where (i) the adsorbed film evaporates or condenses partially, with the excess amount accommodated into the vapor phase,[48] or (ii) the film breaks and forms a sessile droplet.[49] In practice, because we are at a fairly low temperature, close to the wetting transition, and the lateral area is small, the role of these fluctuations is not important.[48,49]

Once a simple coarse-grained measure of adsorption is defined, we set up a simulation box with the CO_2 adsorbing wall at one side and a purely hard repulsive wall at the other side. A grand canonical simulation is then performed at some arbitrarily chosen chemical potential, μ_0 close to coexistence. During the course of the simulation, the total number of molecules fluctuates and we can monitor $P_0(N)$ the probability of observing a given amount of molecules. From this distribution, it is possible to estimate the corresponding probability at coexistence chemical potential, μ_c, through the relation[50,51]

$$P_c(N) = P_0(N)\, e^{\beta(\mu_c - \mu_0)N} \tag{8}$$

where $\beta = 1/k_B T$. In fact, we do not know μ_c, a priori, but we can apply a trick which we have often used in our laboratory that yields excellent results. The idea is that precisely at coexistence, the free energy of a wetting film of sufficient thickness is essentially independent of N. For films away from coexistence, on the contrary, growing liquid films are weighted by a bulk term $e^{\beta(\mu_c-\mu_0)N}$. Therefore, a logarithmic plot of $P_0(N)$ as a function of N becomes a straight line for sufficiently large N, and the slope of that line gives us precisely $\beta(\mu_0 - \mu_c)$, whereby we can estimate μ_c from that slope (see the inset of Figure 2a). This method is approximate to the extent that the substrate interacts with the liquid−vapor interface. However, this interaction is very weak for thick films. For more accurate calculations, the same trick may be performed for a liquid slab placed at the center of a prismatic simulation box with periodic boundary conditions in all three directions, where we have checked that the method produces coexistence chemical potentials with an accuracy comparable with the equal area rule,[47] at much less computational cost. We illustrate this in Figure 2a by comparing the coexistence chemical potentials obtained using this method with the previous results by Wilding and Errington using the equal area rule. As shown in the figure, the method works very accurately all the way from low temperatures to the vicinity of the critical point.[32,47]

Once we know $P_c(N)$, we estimate a coarse-grained interface potential as[44]

$$g(h) = -\frac{k_B T}{A} \ln P_c(N(h)) \tag{9}$$

where we simply exploit the univocal correspondence between N and h that results from the definition in eq 7.

Obviously, the success of this method relies on having a sufficiently accurate probability function $P_c(N)$ over a large range of molecules covering all the way from close to zero adsorption to the formation of thick wetting films. This is generally not an easy task because even at $\mu = \mu_c$, there might be large free energy barriers separating the thin films from the wetting films. To properly sample a prescribed range of molecules, we have employed transition matrix Monte Carlo.[52] This technique allows exploiting the information of rejected insertion/removal attempts to simultaneously build up an accurate probability histogram and tunneling the free energy barriers. The application of this method to the grand canonical ensemble has been largely documented by Errington and co-workers, and we refer the reader to that work for further details.[32,53]

The full line of Figure 2b shows an interface potential calculated as described above. Unfortunately, the definition of the order parameter introduced in eq 7 as an average of $h(\mathbf{x})$ breaks down for films thinner than about 1.5 molecular diameter. Indeed, $h(\mathbf{x})$ as obtained from the ISM relies on defining first of all what liquid molecules are. The criterion that is employed relies on the properties of a bulk liquid so that when the few condensed atoms are all too close to the

DOI: 10.1021/acsomega.7b01650
ACS Omega 2018, 3, 112−123

substrate, the method does no longer work. To fix this, we resort to an alternative definition based on the location of the equimolar dividing surface:

$$(\rho_l - \rho_0)A\hat{h} = N - \rho_v V \tag{10}$$

where ρ_l and ρ_v are the coexistence bulk liquid and vapor densities, respectively. In practice, the only significant difference between $\hat{h}$ and h is a constant mismatch of $\approx 0.30\sigma$, so that $g(\hat{h})$ and $g(h)$ differ by a mere translation. Obviously, we could have simply presented $g(h)$ using the equimolar criterion for h, which is just as good. However, for later comparison with the results for the film height fluctuations, which are best studied with the local order parameter, we need to have the interface potential described on the same footing.

Capillary Wave Spectrum. As mentioned earlier, the surface of a film is never actually flat but rather exhibits local height fluctuations that convey a wealth of information of the surface properties.[15,21,46,54,55] This information may be obtained conveniently from the spectrum of film height fluctuations, $\langle h^2(q)\rangle$, also known as the capillary wave spectrum. To calculate the height fluctuations, it is necessary to define the location of the liquid−vapor interface in the first place. Particularly, it is necessary to estimate the local interface position, $h(\mathbf{x})$, at every point $\mathbf{x}$ of the substrate, for each atomic configuration. Usually, this implies applying some criteria to decide which atoms belong to the liquid phase, followed by a decision as to which of such atoms lie on the surface (pivot atoms).[15,46,54,56,57] This task cannot be done at atomic scale resolution without some degree of arbitrariness.[57] In this work, we have adopted the ISM,[46] which is quite time-consuming but provides results that are very much consistent with the capillary wave theory.[21,46,58,59] The distinct feature of this method is that the pivot atoms are selected iteratively in such a way as to minimize the nominal surface area of the actual interface. This can only be achieved at a high computational cost but allows extending the small wavevector regime of capillary wave theory to atomic scales.[21,22,58−60] This is very important in simulations of finite-size systems because the regime of wavevectors that can be explored is limited to $q_{min} = 2\pi/L_x$, where L_x is the lateral system size.

Having decided the criteria to locate the interface, we perform NVT Monte Carlo simulations as explained above. For each fixed amount of molecules, we select 5×10^4 configurations and obtain the thermal average of the capillary wave fluctuations, $\langle \delta h^2(q)\rangle$. According to the expectations from the capillary wave theory, the inverse Fourier amplitudes of the spectrum for adsorbed fluids with short-range fluid−fluid interactions follow a polynomial in even powers of the wavevector:[61,62]

$$\frac{1}{A\langle |h(\mathbf{q})|^2\rangle} = \beta g''_{cw}(h) + \beta\gamma_{cw}(h)q^2 + \beta\kappa_{cw}(h)q^4 \tag{11}$$

where $g''_{cw}(h)$, $\gamma_{cw}(h)$, and $\kappa_{cw}(h)$ are the coefficients of the polynomial expansion. The subscript cw in the coefficients indicates that we make no a priori assumption as to their physical significance, and the argument h indicates that in the absence of any physical input, we allow them to exhibit, in principle, a film height dependence. Of course, the names of the coefficients do remind us of capillary wave theory expectations, where $g''_{cw}(h) = g''(h)$ is given by the second derivative of the interface potential while the remaining higher order coefficients are constant and obey $\gamma_{cw}(h) = \gamma_{lv}$ and $\kappa_{cw}(h) = \kappa_{lv}$, where γ_{lv} and κ_{lv} are the interface tension and the bending rigidity of the liquid−vapor interface, respectively. Notice that in the study of the capillary wave spectrum, we will use $\beta = 1/k_BT$ as unit of energy.

Fitting an arbitrary function to a polynomial in such a way that the coefficients retain their physical significance is not an easy task. This problem is particularly relevant in this case because eq 11 is, in principle, a limiting law restricted to small wavevectors and indeed the results of the fit depend strongly on the number of data points that is used in the regression.

The strategy we have adopted is as follows. First, we attempt to fit the spectrum for the thickest film. In such cases, we know a priori that g''_{cw}, which decays fast, is very small and we can assume that $g''_{cw} = 0$. Accordingly, $\gamma_{cw}(h) = \gamma_{lv}$ corresponds to the surface tension of a free interface, which we know from independent simulations. With this information at hand, we perform a fit to eq 11 for several sets of points in the low q regime. The largest set that provides a good enough estimate of γ_{lv} from the coefficient $\gamma_{cw}(h)$ determines the number of data points that we will employ in all subsequent fits to the spectrum of thinner films. This corresponds, in our case, to the capillary wave amplitudes $\langle h^2(q)\rangle$ for the five smaller wavevectors, which lie between $q\sigma = 0.62$ and $q\sigma = 1.77$. Having obtained a consistent fit for the thickest film, we then use the parameters so obtained as the initial guess for the next film and proceed iteratively up to the thinnest film studied. This procedure is crucial for the success of the analysis.

RESULTS

Interface Potential and Prewetting Equilibrium. Figure 2b shows the interface potential calculated at a temperature $k_BT = 0.65\epsilon$. Clearly, the interface potential exhibits a pronounced minimum at very small adsorption. However, the minimum is located at surface free energies that are above those corresponding to infinitely thick films. Hence, the minimum is metastable. Yet, the only way for the thick film to grow is by crossing a rather large activation barrier. Films formed with thicknesses greater than those at the maximum, within the region where the interface potential is concave, are stable films that can develop into fully wetting films as coexistence is approached.

The derivative of the interface potential, as described in the Introduction, provides the disjoining pressure isotherm, which is shown in the inset. Disjoining pressures that are positive correspond to the adsorbed films at supersaturation. A horizontal line above 0 represents the states at supersaturation. For sufficiently small saturations, the line crosses three states of small, intermediate, and large adsorption. Out of these three states, the second one at intermediate adsorption corresponds to an unstable state. The thin and thick films are either absolutely or partially stable states. For one single supersaturation obeying the equal area rule under the disjoining pressure isotherm, the thin and thick films may be found in equilibrium.

We checked that our system exhibits the prewetting equilibrium expected from the disjoining pressure isotherm. To this end, we place a layer of molecules on a substrate with a total adsorption in between those expected for the thin and thick states of the prewetting equilibrium and performed lengthy canonical simulations. Our results show that a flat layered "pancake" is equilibrated in the system, whence, showing the coexistence between a thick and a thin adsorbed film, close to a bare substrate (Figure 3). The pancake is

DOI: 10.1021/acsomega.7b01650
ACS Omega 2018, 3, 112−123

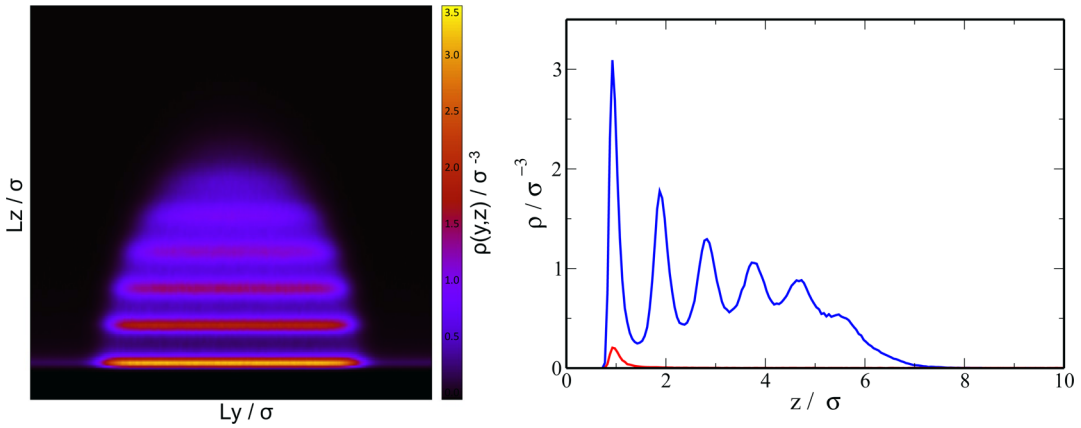

Figure 3. Prewetting equilibrium of a thick adsorbed layer with a thin (almost bare substrate) state. Left: density plot showing the layered structure of a pancake. Right: density cuts across the center of the pancake (blue line) and on the thin state (red line).

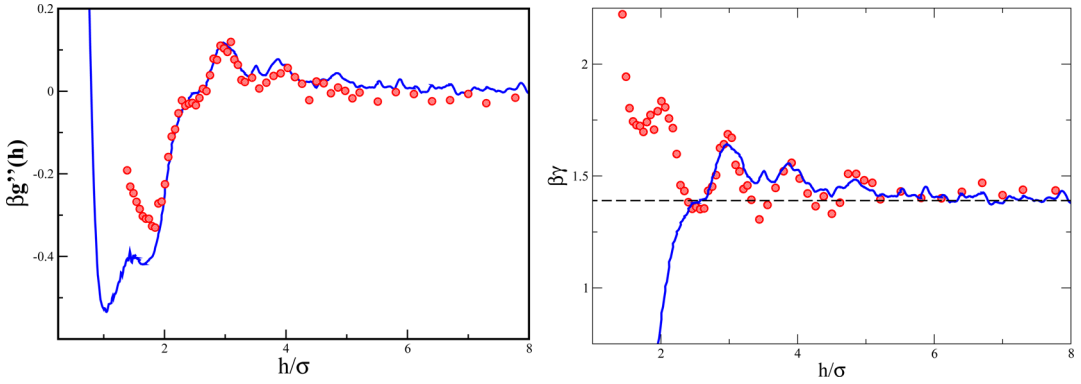

Figure 4. Coefficients of the capillary wave spectrum obtained as a function of film height. Left: second derivative of the interface potential as obtained from the numerical differentiation of $g(h)$ (lines) and a fit to the capillary wave spectrum (symbols). Right: film height-dependent surface tension as obtained from a fit to the capillary wave spectrum. The lines are the results obtained from eq 11, with the adjustable parameter $\xi = 1.46\sigma$.

distinctly different from a droplet because it remains flat on the top and only grows laterally, with the pancake height remaining constant. Similar to a droplet, however, growth of the pancakes is an activated process, which is favored by the surface free energy but penalized by contributions from the line tension along the perimeter of the pancake. Such a free energy, also known as boundary tension, is positive for prewetting films and becomes equal to the line tension precisely at the wetting temperature.[33] Because of this free energy cost, in an open system, the pancake will either grow to a full homogeneous thick film or evaporate to the low adsorption state.

Spectrum of Height Fluctuations. In Figure 4, we show the results obtained from the fit of eq 11 to the capillary wave spectrum for films with thickness ranging from one to nine molecular diameters (symbols).

The left panel shows the zeroth order coefficient of the fit, which, according to eq 11, is equal to the second derivative of the interface potential. Using the results for $g(h)$ obtained by the thermodynamic integration in the previous section (c.f. Figure 2), we can test this prediction of capillary wave theory. The results for $g''(h)$ as obtained from the numerical differentiation of the thermodynamic integration exhibit excellent agreement with the zeroth order coefficient of the capillary wave spectrum all the way from thick films of several-molecular diameter to about only two molecular diameters.

This is a remarkable result because in principle the capillary wave theory is formulated as a low wavevector limit of surface fluctuations. Accordingly, the parameters of the theory, in principle, can be extracted from a fit to eq 11 only in the limit of zero wavevectors. In practice, in our finite-system size simulations, we can only study wavevectors that are limited by the fairly small system size of $L = 10$ molecular diameters. Yet, clearly, the agreement between thermodynamic integration and capillary wave results for $g''(h)$ is excellent down to the adsorbed bilayers. Furthermore, the agreement remains good even in a region where $g''(h)$ is negative, and accordingly, the uniform film is unstable for sufficiently small wavevectors. In practice, in this regime, our finite system sizes turn out to be advantageous because from the theory of spinodal dewetting, we know that films can remain metastable to fluctuations of wavevectors larger than $q^* = \sqrt{\gamma/|g''(h)|}$.[63] Eventually, for thicknesses even smaller than two molecular diameters, the agreement does no longer hold. Essentially, we cannot possibly go beyond this film thickness because the cluster algorithm designed to locate the liquid−vapor surface boundary starts to break down for such thin films. However, an interesting avenue for further exploration would be to extend the method such that it produces a limiting zero film height when the bare substrate is left locally without coverage.

In the right panel of Figure 4, we show the results obtained for the second-order coefficient of the fit of capillary wave fluctuations. According to the classical capillary theory, this coefficient corresponds to the interface tension. In the figure, we can see that thick adsorbed layers exhibit indeed a constant

DOI: 10.1021/acsomega.7b01650
ACS Omega 2018, 3, 112−123

coefficient, which approaches the liquid−vapor interface tension as obtained from independent simulations of the liquid−vapor coexistence.[45] However, for thicknesses below about five molecular diameters, we find that the coefficients of the fit start to develop a clear and strong oscillatory behavior. The classical theory of capillarity does not provide an explanation for this behavior. However, in previous work, we have shown that for adsorbed fluids that are subject to van der Waals interactions, the film thickness dependence of the surface tension as measured from the spectrum of surface fluctuations is related to the disjoining pressure, as indicated in eq 4. Fortunately, we can test this equation readily, performing numerical differentiation of the disjoining pressure isotherm obtained previously (c.f. Figure 2) and using ξ_e, the width of the interface, as an empirical parameter. The results, which are shown as a full line, indicate that the theory is accurate again down to about two and a half molecular layers of thickness.

Below that thickness, unfortunately, the theoretical result of eq 4 seems to break down completely. This is in fact not altogether a surprise because eq 4 is an approximate expression which assumes that the liquid−vapor density profile of the adsorbed film does not change with film thickness. This obviously is a rather coarse approximation but seems to remain robust for very thin films. Eventually, however, a bulk liquid phase does not develop at all, and the approximation breaks down. Unfortunately, a simple analytical expression for $\gamma(h)$ does not seem possible in this regime of small film thickness, where the density profile strongly changes with film thickness.

Despite this difficulty, the results are remarkable because they show that a theory meant to describe the liquid−vapor interface may be used for thin adsorbed interfaces and extrapolated down to thicknesses of almost two molecular diameters, which really is the limit where defining a liquid−vapor interface makes sense.

The good agreement that is found here for a prewetting film is in line with previous results obtained from computer simulations for two related systems[21,22] and with a statistical mechanical theory proposed recently.[23]

Just as the measure of interface tensions in flat liquid films is used in capillary theory to describe curved interfaces via the Young−Laplace equation, we will next try to assess whether the concept of film thickness-dependent surface tensions may be extended to describe the behavior of curved thin interfaces that are present in capillary bridges between spherical colloidal nanoparticles.

APPLICATION TO LIQUID BRIDGES

Capillary forces are able to stick spherical colloids together in the presence of humidity. Because of the presence of vapor, water molecules condense on the nanosphere surface and form a liquid bridge that binds them together.[6]

As long as the nanoparticles remain inert and are not subject to reconstruction, the force required to pull the nanoparticles away is the sum of a structural contribution, mainly due to the packing effects of water molecules, and a capillary force. In the classical approximation for large spherical particles, the capillary force stems exclusively from a bulk pressure difference between the condensed and vapor phases, which is sustained by surface tension. For a pair of wet spherical particles of radius R with a capillary bridge spanning a (small) filling angle β, the force is then simply $F = 2\pi R\gamma_{lv}$, independent of humidity and filling angle.[6] For smaller nanoparticles, the filling angle is no longer small, and the tension along a perimeter of the ring $R\sin(\beta)$ now makes a significant contribution that may even supersede the bulk contribution.[64] In this case, the classical capillary theory is expected to obey the following equation:[65,66]

$$F = 2\pi\gamma_{lv}R\sin(\beta)\left[\sin(\beta+\Theta) + \frac{1}{2}\sin(\beta)\left(\frac{R}{r_m} - \frac{R}{l_m}\right)\right] \quad (12)$$

where r_m and l_m are the equatorial and meridian radii of curvature of the pendular ring, respectively, which depend on the thermodynamic conditions and the distance, D, between the colloids; and Θ is the contact angle of the liquid film on the nanoparticle substrate.

In a recent computer simulation study, the force due to water capillary bridges between two TiO_2 nanoparticles of radius R = 4 nm was studied as a function of nanoparticle distance D.[64] The simulations offer a very convenient tool to study the problem. The measure of force versus distance curves shows clearly a number of large amplitude oscillations (hydration forces that result from the layered water structure), superimposed over a smooth monotonic decay that can be attributed to the capillary forces alone. For very hydrophilic rutile particles similar to the ones considered here, the contact angle turns out to be $\Theta = 0$ in practice and the nanoparticles are always surrounded by a layer of liquid. In this case, by measuring separately the force between the liquid bridge-mediated particles and that found between two equal particles completely immersed in water, it is possible to resolve the structural and capillary contributions to the overall adhesion force and test each separately against theory.[64] As an additional token, the shape of the capillary bridge can be readily calculated from the equilibrium density profile of water molecules. In this way, eq 12 may be tested using the exact geometrical parameters describing the simulated capillary bridge.

Unfortunately, in the study, it was found that the capillary force measured as a function of D did not obey eq 12, even when the correct geometrical parameters obtained in the simulation were used as inputs.

One reason for the discrepancy with classical results is that the nanoparticles are wet by a liquid film with thickness h_e which is not negligible relative to the small nanoparticle radius, R. Accordingly, the Young−Laplace equation is no longer accurate as a means to determine the shape of the capillary bridge. The exact treatment requires solving eq 1, taking into account the role of the film−vapor disjoining pressure explicitly, but simple analytical solutions are only available for large particles.[67] Fortunately, for atomic force microscopy (AFM) tips as small as 10 nm in radius, it has been noticed that the known results for the capillary bridge in the absence of wetting[65] provide a very good approximation for the wet nanoparticles, by merely applying the simple transformations $R \rightarrow R + h_e$ and $D \rightarrow D + 2h_e$ in eq 12.[68,69]

In ref 64, it was noticed that this approximation provides accurate results for the shape of the capillary bridge, but it was found that even using the exact filling angle β obtained from averaged film profiles, the calculated capillary force was smaller than that measured in the computer simulations. Physically, the implication is that the force required to stretch the interface as the nanoparticles are pulled away must be larger than expected. That is, this suggests that γ_{lv} in eq 12 does not fully account for the tangential stress of the adsorbed interface. On the contrary, it was found that by replacing γ_{lv} by an effective humidity-dependent surface tension, γ, larger than γ_{lv}, a very good

DOI: 10.1021/acsomega.7b01650
ACS Omega 2018, 3, 112−123

agreement could be achieved (Figure 5). Such results are consistent with previous observations for the capillary force on AFM tips,[70,71] but an explanation for this increased surface tension is entirely lacking.

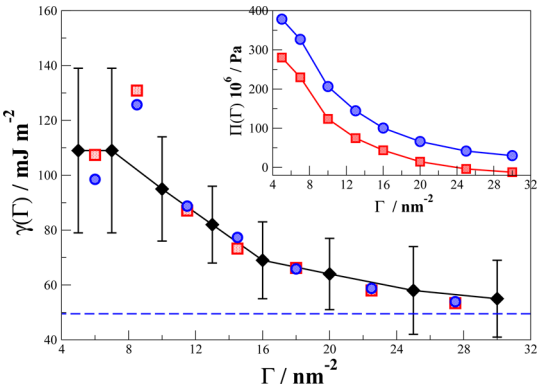

Figure 5. Plot of the film height-dependent surface tension. The filled diamonds are effective surface tensions obtained from a fit of capillary forces to eq 12.[64] The shaded symbols are theoretical predictions from eq 13, using different choices for the disjoining pressure (inset). The red squares correspond to $\Pi(h)$ as estimated for a planar film, using eq 1 with $\kappa = 0$; the blue circles are results for $\Pi(h;R)$ as estimated for a film on the spherical nanoparticle, using eq 1 with $\kappa = 2/(R + h)$. Derivatives of the disjoining pressure are evaluated at the mid points between adjacent data as the slope of the line joining them.

In the light of eq 4, we expect that the humidity of the atmosphere imposes a surface coverage, Γ_e, which can be related to the film height as $\Gamma_e = \rho_l h_e$, with ρ_l being the bulk liquid density of water at coexistence. Because in the simulations, the humidity remains essentially constant as the particles are pulled out, γ remains constant throughout but may become significantly larger than γ_{lv} for sufficiently low coverage. Indeed, it was found that the effective surface tension required to describe $F(D)$ increased as the film coverage or humidity decreased. This provides a qualitative explanation of the observations of ref 64.

We now test whether it is possible to describe quantitatively the empirical surface tensions observed in terms of surface coverage, as

$$\gamma(\Gamma) = \gamma_{lv} - \rho_l^* \xi_e^{\,2} \frac{d\Pi}{d\Gamma} \tag{13}$$

which is simply a rewrite of eq 4 in terms of Γ.

First, we need to asses the disjoining pressure isotherm corresponding to the adsorption of water on spherical TiO_2 nanoparticles.

Assuming that the coverage of water on the spherical nanoparticles is similar to that on a flat substrate, where $\kappa = 0$, we obtain from eq 1 $\Pi(\Gamma) = p_v(\mu) - p_l(\mu)$,[6,22,72,73] where p_v and p_l denote the bulk pressures of vapor and liquid phases at the chemical potential of the water atmosphere, respectively. For incompressible liquids with a negligible vapor pressure, we can write

$$\Pi(\Gamma) = -k_B T \rho_l^* \ln\left(\frac{p_v(\Gamma)}{p_v^*}\right) \tag{14}$$

where p_v^* is the vapor pressure of coexisting planar phases (volumetric phase coexistence). Fortunately, from the reported ratio $p_v(\Gamma)/p_v^*$, we are able to calculate the full disjoining pressure isotherm, as shown in Figure 5.

In practice, it is known that the finite size and curved surface of the nanoparticles considerably impact on the disjoining pressure.[74−77] Accordingly, we must distinguish $\Pi(\Gamma)$, pertaining to a flat substrate, from $\Pi(\Gamma;R)$, corresponding to the disjoining pressure of the liquid film on the curved substrate. Again, we can also assess $\Pi(\Gamma;R)$ from eq 1, by noticing that in the sides opposite to the liquid bridge, the curvature is essentially given by $\kappa = 2/(R + h_e)$. Hence,

$$\Pi(\Gamma; R) = \Pi(\Gamma) + \frac{2\gamma(\Gamma)}{R + h_e} \tag{15}$$

As expected for systems with van der Waals forces, we find for $h < R$ that $\Pi(\Gamma;R)$ is larger than $\Pi(\Gamma)$ but the slopes remain similar. Indeed, from theoretical considerations, it is found that in a regime $h/R < 1$, $\Pi(\Gamma;R)$ differs from $\Pi(\Gamma)$ by a factor $(1 + 1/2 \cdot h_e/R)$, which remains small for all ranges of surface coverage studied here.[74,75,77]

Having the disjoining pressure at hand, we could apply eq 13, using $\xi_e^{\,2}$ as an adjustable parameter. Instead, we recall that ξ_e is a measure of the interface width.[23] Accordingly, we can obtain this parameter ab initio from the results of the liquid−vapor interface profile of the TIP3P model used in the simulations.[78,79] Using fits from ref 79 for the interface profile for the TIP3P model precisely at the temperature of interest $T = 300$ K, we find $\gamma_{lv} = 49.5$ mJ/m^2 and $\rho_l \xi_e^{\,2} = 2.3$ nm^{-1}.[a] We use this result together with $\Pi(h)$ to predict $\gamma(\Gamma)$, as shown in Figure 5. The agreement is impressive, given the absence of any adjustable parameter. In fact, the definition of an interface width is slightly ambiguous and depends on a number of choices so that the optimal result for $\rho_l \xi_e^{\,2}$ obtained without fitting must be considered as slightly coincidental. This serves, nevertheless, to highlight that the order of magnitude of the fitting parameter ξ_e is indeed dictated by the interface width as expected from the theoretical considerations.[21−23] We can also estimate $\gamma(\Gamma)$ employing $\Pi(\Gamma;R)$ instead of $\Pi(\Gamma)$ in eq 13, using now a corrected value for $\rho_l \xi_e^{\,2}$ that is obtained from the average ratio of $\Pi(h)/\Pi(\Gamma;R)$. The results shown in the figure also provide a very good agreement for the observed film height-dependent surface tension $\gamma(\Gamma)$.

DISCUSSION

Despite the very good agreement observed, we must take these results with some caution.

First, Tolman corrections indicate that the ratio between surface tensions for curved and flat interfaces varies as $1 - 2\delta/R$, where δ is the Tolman length and R is the radius of the interface. We are not aware of the measurements of the Tolman length for the TIP3P model used in the simulations, but simulations of the mW and TIP4P/2005 models suggest a small and negative Tolman length of about $\delta \approx -0.05$ nm.[80] Such a small value is in line with theoretical estimates, which indicates that the Tolman length is given by the difference between the bulk correlation lengths of liquid and vapor phases.[81] Taking into account that the radius of the liquid−vapor envelope changes in this study from 2.2 nm at the lowest humidity and 2.6 nm at the highest, we find that Tolman corrections could, in principle, be as much as 5% but, on the other hand, can only account for a variation of the surface tension of less than 2% within the range of humidities considered. On the contrary, the surface tensions analyzed here

DOI: 10.1021/acsomega.7b01650
ACS Omega 2018, 3, 112−123

exhibit a variation of about a factor of 2 in this range. Therefore, whatever the extent of the correction from curvature effects, it seems it has too weak size dependence to account for the large change in surface tension observed here.

Other curvature corrections, such as a possible ln R term resulting from the van der Waals interactions,[75,77] cannot explain the large variations observed here for similar reasons. Indeed, h_e always remains considerably smaller than R so that the change of curvature with humidity is only of order h_e/R, and one can hardly expect this to provide such a large humidity dependence as observed for $\gamma(\Gamma)$ (nor is there a reason to suspect such dependency is to follow $d\Pi/d\Gamma$).

A far more difficult issue refers to the applicability of eq 12. This equation assumes that the net force stems from a bulk pressure effect $\Delta p R^2 \sin^2 \beta$, producing effectively a force on the projected area, $R^2 \sin^2 \beta$, and a surface tension effect $\gamma_{lv} R \sin^2 \beta$ on the perimeter of that surface. Both contributions may be expressed in terms of γ_{lv} by the use of $\Delta p = 2\gamma_{lv}\kappa$. The empirical surface tension measured from simulations is obtained by replacing γ_{lv} with the humidity-dependent $\gamma(\Gamma)$. This seems rather plausible for the surface contribution stemming from the tension at the rim of the bridge on the sphere because there the film height is very close to h_e. However, it is less justified to do this for the bulk pressure contribution because the pressure drop is measured in the equatorial plane of the capillary bridge, where the influence of the disjoining pressure should be smaller and may not justify a tension significantly larger than γ_{lv}. On the other hand, if the disjoining pressure were not negligible at the equator of the bridge, then the full Young−Laplace−Derjaguin equation should be employed to estimate the pressure drop.

Furthermore, we notice that in ref 64 as well as in other theoretical studies,[67−71,82] the disjoining pressure was considered either implicitly or explicitly as a means to assess the size of the pendular bridge, yet the classical force balance of eq 12 was employed in all cases. However, it must be born in mind that such a result is obtained for systems where the liquid phase has a uniform and constant pressure as dictated by the Young−Laplace equation. For smaller systems with wetting films, where the disjoining pressure is introduced, the pressure of the condensed phase does not remain uniform throughout. In fact, at the poles of the spheres, the film pressure is larger than that of the vapor phase, whereas in the bridge, it becomes smaller. A full account of the capillary force in this very complex situation seems to be lacking, but the results reported here make such a study desirable to fully elucidate the significance of the film height-dependent surface tension observed by Laube et al. and discussed here.

As a final word of caution, we note that the approach studied here holds provided the nanoparticles remain inert while approaching each other. For sufficiently small distances and particularly for such small distances that a single water layer does not fit in the space between, the nanoparticles could undergo surface reconstruction and even fully chemical adhesion, and such a complicated scenario is completely beyond the capabilities of this approach.

CONCLUSIONS

In colloidal science, the Young−Laplace equation is employed ubiquitously to study curved interfaces on the micrometer scale. Beyond this scale down to decades of nanometers, one must account for first-order corrections to the fluid−substrate interactions via the disjoining pressure, as in the Young−Laplace−Derjaguin equation, eq 1. In this paper, we have shown that approaching the limit of very thin films fully accounting for fluid−substrate interactions requires taking into consideration a modified surface tension, which can be more than double γ_{lv} for films of about 1 nm thickness. Fortunately, we have shown that the resulting film height-dependent surface tension may be described in terms of the known disjoining pressure. With this addition, the results of capillarity theory meant for the micrometer range may be apparently extrapolated down to the limit where a "film" is meaningful provided the short distances do not trigger significant covalent interactions between the surfaces. A detailed analysis on the force required to pull small nanoparticles subject to inhomogeneous pressure fields seems desirable to fully asses the significance of this observation.

METHODS

Unless otherwise stated, we simulate adsorbed films in a prismatic box, with sides of size $L_x = L_y = 10\sigma$ and $L_z = 50\sigma$. An adsorbing wall mimicking CO_2 is placed at one side of the box perpendicular to the z direction, and a purely repulsive wall is placed in the opposite side. Canonical Monte Carlo simulations are performed, which implement both ordinary center of mass metropolis translations and configurational biased translations of a molecule chosen at random to a random position on the simulation box.[83] Simulations are organized in cycles, with a cycle consisting of as many MC attempts as molecules in the system. The trial attempts described above are performed in a ratio of 1:1. Typical averages are collected over five batches of 10^7 cycles.

To precisely locate the triple point, we proceeded as follows. First, we simulated the liquid−vapor coexistence curve in a wide range of temperatures between $k_BT = 1.00\epsilon$ and $k_BT = 0.50\epsilon$, well below the expected triple point using the method of direct coexistence. Our results are in good agreement with ref 84. For higher temperatures, the direct coexistence method is less reliable because the large bulk correlation lengths result in very broad interfaces. This precludes an accurate determination of the bulk densities in our finite system ($L_x = L_y = 10\sigma$ and $L_z = 50\sigma$) because the density profile hardly attains bulk values. For this reason, we resorted to multicanonical and histogram reweighting simulations combined with finite-size scaling.[85−87] We checked that our results are in excellent agreement with previous calculations for the same model.[47]

In a second stage, we estimated the solid−vapor coexistence curve by direct coexistence. A perfect face-centered cubic lattice of atoms was arranged in a cubic box with sides of $L_x = L_y = L_z = 10\sigma$. The system was then simulated using NPT Monte Carlo simulations at $k_BT = 0.50\sigma$ and 0 pressure. After equilibration, we performed a cell expansion, leaving the equilibrated $L_x = L_y$ sides fixed and increasing L_z up to 50σ. This leaves a condensed solid slab in the center of the simulation box, surrounded by the vapor phase. Simulations were then performed in the canonical ensemble, and the vapor densities were evaluated from the equilibrated density profile. The final configuration was employed as the initial state for a new run at higher temperatures, and the process was repeated until the solid phase melts.

Because the vapor−solid interface of the LJ fluid exhibits surface melting, we were unable to observe any significant overheating of the solid phase. To accurately locate the triple point, we fitted the vapor densities, $\rho_v(T)$, of the solid−vapor and liquid−vapor branches to a polynomial in the temperature and estimated the triple-point temperature as the intercept of

DOI: 10.1021/acsomega.7b01650
ACS Omega 2018, 3, 112−123

both curves, yielding $k_B T_t = 0.631\epsilon$ and $\sigma^3\rho_v(T_t) = 0.00155$. This result lies between the two available results for the truncated and shifted LJ potentials with equal cutoff, which unfortunately differ significantly. Toxvaerd performed direct coexistence simulations and estimated $k_B T_t = 0.618\epsilon$,[34] whereas van Meel et al. performed free energy calculations and suggested $k_B T \approx 0.65\epsilon$.[39]

To complete the phase diagram, we estimated the triple-point pressure from the above density, using a virial expansion, with virial coefficients as determined from Sun and Teja.[88] The resulting triple-point pressure and temperature were employed thereof to estimate the coexistence liquid and solid densities in NPT simulation. The results for the enthalpies and densities of the condensed phases were then used as inputs to extrapolate the coexistence pressure at higher temperatures, using the Clapeyron equation. This process so iterated is known as the Gibbs−Duhem integration method[89] and allowed us to estimate the solid−liquid coexistence line up to $k_B T = 1.0\epsilon$.

AUTHOR INFORMATION

Corresponding Author

*E-mail: lgmac@quim.ucm.es. Phone: +34 (0)91 394 42 13. Fax +34 (0)91 394 41 35 (L.G.M.).

ORCID

Luis G. MacDowell: 0000-0003-1900-1241

Andrés Guerrero-Martinez: 0000-0001-8576-2896

Notes

The authors declare no competing financial interest.

ACKNOWLEDGMENTS

We would like to thank Nebil A. Katcho for invaluable assistance. L.G.M. would like to thank H. Kusumaatmaja and C. Semprebon for helpful discussions and A. Archer and D. Sibley for an enjoyable stay at the University of Loughborough. A travel grant from the Spanish Ministerio de Educación, Cultura y Deporte, Programa Salvador de Madariaga (Ref. PRX17/00460) is gratefully acknowledged. The authors would also like to acknowledge the financial support from the Spanish Ministerio de Economia y Competitividad under grant MAT-2014-59678-R.

ADDITIONAL NOTE

[a]Notice that the definition of interface width is not without ambiguity. In refs 22 and 23, we show that eq 13 follows by assuming that the interface profile may be fit to an error function of width ξ_e. In practice, in ref 79, the authors perform fits of the interface profile in terms of hyperbolic tangent function of width ξ_t but report results of the so-called 10−90 width, $t_{10-90} = 2.2/2\xi_t$. Using their result $t_{10-90} = 0.378$ nm and the relation $\xi_e = \pi^3/24\cdot\xi_t^2$,[78] we find $\xi_e^2 = 0.070$ nm^2. This, with $\rho_l = 0.980$ g cm^{-3},[79] yields the reported value $\rho_l\xi_e^2 = 2.3$ nm^{-1}.

REFERENCES

(1) Haimov, B.; Iakovlev, A.; Glick-Carmi, R.; Bloch, L.; Rich, B. B.; Müller, M.; Pokroy, B. Kinetics of nano-scale self-assembly measured on liquid drops by macroscopic optical tensiometry: from mercury to water and fluorocarbons. *J. Am. Chem. Soc.* **2016**, *138*, 2585−2591.

(2) Yunker, P. J.; Still, T.; Lohr, M. A.; Yodh, A. G. Suppression of the coffee-ring effect by shape-dependent capillary interactions. *Nature* **2011**, *476*, 308−311.

(3) Coelho, J. P.; González-Rubio, G.; Delices, A.; Barcina, J. O.; Salgado, C.; Ávila, D.; Peña-Rodríguez, O.; Tardajos, G.; Guerrero-Martínez, A. Polyrotaxane-Mediated Self-Assembly of Gold Nanospheres into Fully Reversible Supercrystals. *Angew. Chem., Int. Ed.* **2014**, *53*, 12751−12755.

(4) Maestro, A.; Guzmán, E.; Ortega, F.; Rubio, R. G. Contact angle of micro- and nanoparticles at fluid interfaces. *Curr. Opin. Colloid Interface Sci.* **2014**, *19*, 355−367.

(5) Kusumaatmaja, H.; Lipowsky, R. Equilibrium Morphologies and Effective Spring Constants of Capillary Bridges. *Langmuir* **2010**, *26*, 18734−18741.

(6) Israelachvili, J. N. *Intermolecular and Surfaces Forces*, 3rd ed.; Academic Press: London, 1991; pp 1−674.

(7) de Gennes, P. G.; Brochard-Wyart, F.; Quéré, D. *Capillarity and Wetting Phenomena*; Springer: New York, 2004; pp 1−292.

(8) Boruvka, L.; Neumann, A. W. Generalization of the classical theory of capillarity. *J. Chem. Phys.* **1977**, *66*, 5464−5476.

(9) Rowlinson, J.; Widom, B. *Molecular Theory of Capillarity*; Clarendon: Oxford, 1982.

(10) Deryagin, B. V. Modern State of the Investigation of Long-Range Surface Forces. *Langmuir* **1987**, *3*, 601−606.

(11) Philip, J. R. Unitary Approach to Capillary Condensation and Adsorption. *J. Chem. Phys.* **1977**, *66*, 5069−5075.

(12) Sharma, A. Equilibrium Contact Angles and Film Thicknesses in the Apolar and Polar Systems: Role of Intermolecular Interactions in Coexistence of Drops with Thin Films. *Langmuir* **1993**, *9*, 3580−3586.

(13) Goldenfeld, N. *Lectures on Phase Transitions and the Renormalization Group*; Perseus Books: Reading, MA, 1992; pp 1−394.

(14) Evans, R. The nature of the liquid-vapour interface and other topics in the statistical mechanics of non-uniform, classical fluids. *Adv. Phys.* **1979**, *28*, 143−200.

(15) Werner, A.; Müller, M.; Schmid, F.; Binder, K. Effect of Long-Range Forces on the Interfacial Profiles in Thin Binary Polymer Films. *J. Chem. Phys.* **1999**, *110*, 1221−1229.

(16) MacDowell, L. G.; Benet, J.; Katcho, N. A.; Palanco, J. M. G. Disjoining Pressure and the Film-Height-Dependent Surface Tension of Thin Liquid Films: New Insight from Capillary Wave Fluctuations. *Adv. Colloid Interface Sci.* **2014**, *206*, 150−171.

(17) Pershan, P. S.; Schlossman, M. *Liquid Surfaces and Interfaces: Synchrotron X-ray Methods*; Cambridge University Press: Cambridge, 2012; pp 1−311.

(18) Doerr, A. K.; Tolan, M.; Prange, W.; Schlomka, J.-P.; Seydel, T.; Press, W.; Smilgies, D.; Struth, B. Observation of Capillary Waves on Liquid Thin Films from Mesoscopic to Atomic Length Scales. *Phys. Rev. Lett.* **1999**, *83*, 3470−3473.

(19) Heilmann, R. K.; Fukuto, M.; Pershan, P. S. Quenching of Capillary Waves in Composite Wetting Films from a Binary Vapor: An X-Ray Reflectivity Study. *Phys. Rev. B: Condens. Matter Mater. Phys.* **2001**, *63*, 205405.

(20) Fukuto, M.; Gang, O.; Alvine, K. J.; Pershan, P. S. Capillary wave fluctuations and intrinsic widths of coupled fluid-fluid interfaces: An x-ray scattering study of a wetting film on bulk liquid. *Phys. Rev. E: Stat., Nonlinear, Soft Matter Phys.* **2006**, *74*, 031607.

(21) MacDowell, L. G.; Benet, J.; Katcho, N. A. Capillary Fluctuations and Film-Height-Dependent Surface Tension of an Adsorbed Liquid Film. *Phys. Rev. Lett.* **2013**, *111*, 047802.

(22) Benet, J.; Palanco, J. G.; Sanz, E.; MacDowell, L. G. Disjoining Pressure, Healing Distance, and Film Height Dependent Surface Tension of Thin Wetting Films. *J. Phys. Chem. C* **2014**, *118*, 22079−22089.

(23) MacDowell, L. G. Capillary Wave Theory of Adsorbed Liquid Films and the Structure of the Liquid-Vapor Interface. *Phys. Rev. E: Stat., Nonlinear, Soft Matter Phys.* **2017**, *96*, 022801.

(24) Bernardino, N. R.; Parry, A. O.; Rascón, C.; Romero-Enrique, J. M. Derivation of a Nonlocal Interfacial Model for 3D Wetting in an External Field. *J. Phys.: Condens. Matter* **2009**, *21*, 465105.

(25) Finn, J. E.; Monson, P. A. Adsorption Equilibria in an Isobaric Ensemble. *Mol. Phys.* **1988**, *65*, 1345−1361.

(26) Finn, J. E.; Monson, P. A. Prewetting at a Solid−Fluid Interface via Monte Carlo Simulation. *Phys. Rev. A: At., Mol., Opt. Phys.* **1989**, *39*, 6402−6408.

DOI: 10.1021/acsomega.7b01650
ACS Omega 2018, 3, 112−123

(27) Sokolowski, S.; Fischer, J. Wetting Transitions at the Argon-Solid-CO2 Interface: Molecular-Dynamics Studies. *Phys. Rev. A: At., Mol., Opt. Phys.* **1990**, *41*, 6866−6870.
(28) Fan, Y.; Monson, P. A. Further Studies of Prewetting Transitions via Monte Carlo Simulations. *J. Chem. Phys.* **1993**, *99*, 6897−6906.
(29) Bojan, M. J.; Stan, G.; Curtarolo, S.; Steele, W. A.; Cole, M. W. Wetting transitions of Ne. *Phys. Rev. E: Stat. Phys., Plasmas, Fluids, Relat. Interdiscip. Top.* **1999**, *59*, 864−873.
(30) Sweatman, M. B. Weighted density-functional theory for simple fluids: Prewetting of a Lennard-Jones fluid. *Phys. Rev. E: Stat., Nonlinear, Soft Matter Phys.* **2001**, *65*, 011102.
(31) Shi, W.; Zhao, X.; Johnson, J. K. Phase transitions of adsorbed fluids computed from multiple-histogram reweighting. *Mol. Phys.* **2002**, *100*, 2139−2150.
(32) Errington, J. R. Prewetting Transitions for a Model Argon on Solid Carbon Dioxide System. *Langmuir* **2004**, *20*, 3798−3804.
(33) Errington, J. R.; Wilbert, D. W. Prewetting Boundary Tensions from Monte Carlo Simulation. *Phys. Rev. Lett.* **2005**, *95*, 226107.
(34) Toxvaerd, S. Molecular Dynamics Simulation of Prewetting. *J. Phys. Chem. C* **2007**, *111*, 15620−15624.
(35) Ebner, C.; Saam, W. F. New Phase Transition in Thin Argon Films. *Phys. Rev. Lett.* **1977**, *38*, 1486−1489.
(36) Velasco, E.; Tarazona, P. Comment on "Prewetting at a solid-fluid interface via Monte Carlo simulation". *Phys. Rev. A: At., Mol., Opt. Phys.* **1990**, *42*, 2454−2457.
(37) Agrawal, R.; Kofke, D. Thermodynamic and Structural Properties of Model Systems at Solid-Fluid Coexistence. II. Melting and Sublimation of the Lennard-Jones System. *Mol. Phys.* **1995**, *85*, 43−59.
(38) Mastny, E. A.; de Pablo, J. J. Melting line of the Lennard-Jones system, infinite size, and full poten tial. *J. Chem. Phys.* **2007**, *127*, 104504.
(39) van Meel, J. A.; Page, A. J.; Sear, R. P.; Frenkel, D. Two-step vapor-crystal nucleation close below triple point. *J. Chem. Phys.* **2008**, *129*, 204505.
(40) Pandit, R.; Fisher, M. E. Wetting Transitions Near Bulk Triple Points. *Phys. Rev. Lett.* **1983**, *51*, 1772−1775.
(41) Mistura, G.; Ancilotto, F.; Bruschi, L.; Toigo, F. Wetting of Argon on CO2. *Phys. Rev. Lett.* **1999**, *82*, 795−798.
(42) Sukhatme, K. G.; Rutledge, J. E.; Taborek, P. Wetting near Triple Points. *Phys. Rev. Lett.* **1998**, *80*, 129−132.
(43) Bruschi, L.; Mistura, G. Triple−point Wetting of Argon and Methane on Gold. *Phys. Rev. B: Condens. Matter Mater. Phys.* **2001**, *61*, 4941−4947.
(44) MacDowell, L. G.; Müller, M. Adsorption of Polymers on a Brush: Tuning the Order of the Wetting Transition. *J. Chem. Phys.* **2006**, *124*, 084907.
(45) de Gregorio, R.; Benet, J.; Katcho, N. A.; Blas, F. J.; MacDowell, L. G. Semi-Infinite Boundary Conditions for the Simulation of Interfaces: The Ar/CO2(s) Model Revisited. *J. Chem. Phys.* **2012**, *136*, 104703.
(46) Chacón, E.; Tarazona, P. Characterization of the Intrinsic Density Profiles for Liquid Surfaces. *J. Phys.: Condens. Matter* **2005**, *17*, S3493−S3498.
(47) Wilding, N. B. Critical−Point and Coexistence−Curve Properties of the Lennard-Jones Fluid: A Finite−Size Scaling Study. *Phys. Rev. E: Stat. Phys., Plasmas, Fluids, Relat. Interdiscip. Top.* **1995**, *52*, 602−611.
(48) Fernández, E. M.; Chacón, E.; Tarazona, P. Thickness and Fluctuations of Free and Adsorbed Liquid Films. *Phys. Rev. E: Stat., Nonlinear, Soft Matter Phys.* **2011**, *84*, 205435.
(49) MacDowell, L. G. Computer Simulation of Interface Properties: Towards a First Principle Description of Complex Interfaces? *Eur. Phys. J.: Spec. Top.* **2011**, *197*, 131−145.
(50) Müller, M.; MacDowell, L. G. Interface and Surface Properties of Polymer Solutions: Monte Carlo Simulations and Self-Consistent Field Theory. *Macromolecules* **2000**, *33*, 3902−3923.
(51) MacDowell, L. G.; Müller, M.; Binder, K. How do Droplets on a Surface Depend on the System size? *Colloids Surf., A* **2002**, *206*, 277−291.
(52) Fitzgerald, M.; Picard, R. R.; Silver, R. N. Canonical transition probabilities for adaptive Metropolis stimulation. *Europhys. Lett.* **1999**, *46*, 282−287.
(53) Grzelak, E. M.; Errington, J. R. Computation of Interfacial Properties via Grand Canonical Transition Matrix Monte Carlo simulation. *J. Chem. Phys.* **2008**, *128*, 014710.
(54) Benjamin, I. Theoretical study of the water/1,2-dichloroethane interface: Structure, dynamics, and conformational equilibria at the liquid−liquid interface. *J. Chem. Phys.* **1992**, *97*, 1432−1445.
(55) Müller, M.; MacDowell, L. G. Wetting of Polymer Liquids: Monte Carlo Simulations and Self Consistent Field Calculations. *J. Phys.: Condens. Matter* **2003**, *15*, R609−R653.
(56) Usabiaga, F. B.; Duque, D. Applications of computational geometry to the molecular simulation of interfaces. *Phys. Rev. E: Stat., Nonlinear, Soft Matter Phys.* **2009**, *79*, 046709.
(57) Jorge, M.; Jedlovszky, P.; Cordeiro, M. N. D. S. A Critical Assessment of Methods for the Intrinsic Analysis of Liquid Interfaces. 1. Surface Site Distributions. *J. Phys. Chem. C* **2010**, *114*, 11169−11179.
(58) Fernández, E. M.; Chacón, E.; Tarazona, P.; Parry, A. O.; Rascón, C. Intrinsic Fluid Interfaces and Nonlocality. *Phys. Rev. Lett.* **2013**, *111*, 096104.
(59) Chacón, E.; Fernández, E. M.; Tarazona, P. Effect of Dispersion Forces on the Capillary-Wave Fluctuations of Liquid Surfaces. *Phys. Rev. E: Stat., Nonlinear, Soft Matter Phys.* **2014**, *89*, 042406.
(60) Fernández, E. M.; Chacón, E.; Tarazona, P. Capillary Waves Spectrum at Adsorbed Liquid Films. *Phys. Rev. B: Condens. Matter Mater. Phys.* **2012**, *86*, 085401.
(61) Mecke, M.; Winkelmann, J.; Fischer, J. Molecular Dynamics Simulations of the Liquid−Vapor Interface: Binary Mixtures of Lennard-Jones Fluids. *J. Chem. Phys.* **1999**, *110*, 1188−1194.
(62) Blokhuis, E. M. On the Spectrum of Fluctuations of a Liquid Surface: From the Molecular Scale to the Macroscopic Scale. *J. Chem. Phys.* **2009**, *130*, 014706.
(63) Vrij, A. Possible Mechanism for the Spontaneous Rupture of Thin, Free Liquid Films. *Discuss. Faraday Soc.* **1966**, *42*, 23−33.
(64) Laube, J.; Salameh, S.; Kappl, M.; Mädler, L.; Ciacchi, L. C. Contact Forces between TiO2 Nanoparticles Governed by an Interplay of Adsorbed Water Layers and Roughness. *Langmuir* **2015**, *31*, 11288−11295.
(65) Orr, F. M.; Scriven, L. E.; Rivas, A. P. Pendular Rings Between Solids: Meniscus Properties and Capillary Forces. *J. Fluid Mech.* **1975**, *67*, 723−742.
(66) Butt, H.-J.; Kappl, M. Normal Capillary Forces. *Adv. Colloid Interface Sci.* **2009**, *146*, 48−60.
(67) Charlaix, E.; Crassous, J. Adhesion forces between wetted solid surfaces. *J. Chem. Phys.* **2005**, *122*, 184701.
(68) Asay, D. B.; de Boer, M. P.; Kim, S. H. Equilibrium Vapor Adsorption and Capillary Force: Exact Laplace-Young Equation Solution and Circular Approximation Approaches. *J. Adhes. Sci. Technol.* **2010**, *24*, 2363−2382.
(69) Crassous, J.; Ciccotti, M.; Charlaix, E. Capillary Force between Wetted Nanometric Contacts and Its Application to Atomic Force Microscopy. *Langmuir* **2011**, *27*, 3468−3473.
(70) Asay, D. B.; Kim, S. H. Effects of adsorbed water layer structure on adhesion force of silicon oxide nanoasperity contact in humid ambient. *J. Chem. Phys.* **2006**, *124*, 174712.
(71) Asay, D. B.; Kim, S. H. Molar Volume and Adsorption Isotherm Dependence of Capillary Forces in Nanoasperity Contacts. *Langmuir* **2007**, *23*, 12174−12178.
(72) Bhatt, D.; Newman, J.; Radke, C. J. Molecular Simulation of Disjoining-Pressure Isotherms for Free Liquid, Lennard-Jones Thin Films. *J. Phys. Chem. B* **2002**, *106*, 6529−6537.
(73) Han, M. Disjoining Properties of Ne and Ar on Graphite Surface. *Colloids Surf., A* **2008**, *317*, 679−686.

DOI: 10.1021/acsomega.7b01650
ACS Omega 2018, 3, 112−123

(74) Gelfand, M. P.; Lipowsky, R. Wetting on cylinders and spheres. *Phys. Rev. B: Condens. Matter Mater. Phys.* **1987**, *36*, 8725−8735.
(75) Bieker, T.; Dietrich, S. Wetting of curved surfaces. *Phys. A* **1998**, *252*, 85−137.
(76) Bryk, P.; Roth, R.; Mecke, K. R.; Dietrich, S. Hard Sphere Fluids in Contact with Curved Substrates. *Phys. Rev. E: Stat., Nonlinear, Soft Matter Phys.* **2003**, *68*, 031602.
(77) Nold, A.; Malijevský, A.; Kalliadasis, S. Wetting on a spherical wall: Influence of liquid-gas interfacial properties. *Phys. Rev. E: Stat., Nonlinear, Soft Matter Phys.* **2011**, *84*, 021603.
(78) Ismail, A. E.; Grest, G. S.; Stevens, M. J. Capillary waves at the liquid-vapor interface and the surface tension of water. *J. Chem. Phys.* **2006**, *125*, 014702.
(79) Vega, C.; de Miguel, E. Surface tension of the most popular models of water by using the test-area simulation method. *J. Chem. Phys.* **2007**, *126*, 154707.
(80) Joswiak, M. N.; Do, R.; Doherty, M. F.; Peters, B. Energetic and entropic components of the Tolman length for mW and TIP4P/2005 water nanodroplets. *J. Chem. Phys.* **2016**, *145*, 204703.
(81) Iwamatsu, M. The Surface Tension and Tolman's Length of a Drop. *J. Phys.: Condens. Matter* **1994**, *6*, L173−L177.
(82) Dobbs, H. T.; Darbellay, G. A.; Yeomans, J. M. Capillary Condensation Between Spheres. *Europhys. Lett.* **1992**, *18*, 439.
(83) MacDowell, L. G. Termodinámica Estadística de Moléculas Flexibles: Teoría y Simulación. Ph.D. Thesis, Universidad Complutense de Madrid, 2000.
(84) Trokhymchuk, A.; Alejandre, J. Computer Simulations of Liquid/Vapor Interface in Lennard-Jones Fluids: Some Questions and Answers. *J. Chem. Phys.* **1999**, *111*, 8510−8523.
(85) Berg, B. A.; Neuhaus, T. Multicanonical Ensemble: A New Approach to Simulate First-Order Phase Transitions. *Phys. Rev. Lett.* **1992**, *68*, 9−12.
(86) Ferrenberg, A. M.; Swendsen, R. H. Optimized Monte Carlo Data Analysis. *Phys. Rev. Lett.* **1989**, *63*, 1195−1198.
(87) Müller, M.; Wilding, N. B. *Phys. Rev. E* **1994**, *57*, 2076.
(88) Sun, T.; Teja, A. S. An Equation of State for Real Fluids Based on the Lennard-Jones Potential. *J. Phys. Chem.* **1996**, *100*, 17365−17372.
(89) Kofke, D. A. Direct Evaluation of Phase Coexistence by Molecular Simulation via Integration Along the Saturation Line. *J. Chem. Phys.* **1993**, *98*, 4149−4162.

DOI: 10.1021/acsomega.7b01650
ACS Omega 2018, 3, 112−123